AIAA JOURNAL
Vol. 51, No. 1, January 2013

# Real-Time Estimation of Time-Varying Bending Modes Using Fiber Bragg Grating Sensor Arrays

Hao Jiang,* Bartel van der Veek,† Daniel Kirk,‡ and Hector Gutierrez§
*Florida Institute of Technology, Melbourne, Florida 32901*

DOI: 10.2514/1.J051702

**An important challenge in launch vehicle simulation and control is created by the time-varying mass and inertia of the vehicle, as well as the consequent changes in modal frequencies and modal shapes of the structure as propellant is exhausted. Estimating modal information from a limited number of onboard sensors is inadequate for attitude control of a launch vehicle in real time, and the use of additional conventional sensors is unwarranted because of the mass penalty and complexity. This limitation has forced mission planners to base vehicle control schemes on pre-calculated modal information from finite element models. Recent advances in fiber Bragg grating (FBG) sensor technology enable locating a large number of sensing elements along a rocket's structure with a negligible mass penalty. This opens the path for real-time modal estimation and control. This paper presents a novel approach for the real-time estimation of mode shapes on a variable mass structure using FBG sensor arrays. The method is validated by comparing estimated modal shapes to both numerical predictions and experimental results from a vertical cantilever beam in which a step change in mass of the beam is introduced. The results show that the first three mode shapes of the beam can be estimated in real time using strain measurements from a FBG sensor array sampled at 1 kHz. Sensitivity and estimation error based on the number of FBG sensors used is also presented.**

Downloaded by STANFORD UNIVERSITY on March 24, 2013 | http://arc.aiaa.org | DOI: 10.2514/1.J051702

## Nomenclature

| | | |
|---|---|---|
| $C_1$ | = | fiber Bragg grating gage constant 1, 6.156 $\mu$m/m/°C at 22 °C |
| $C_2$ | = | fiber Bragg grating gage constant 2, 0.70 $\mu$m/m/°C at 22 °C |
| $\mathrm{CTE}_s$ | = | Coefficient of thermal expansion of test specimen 1, 23.6 $\mu$m/m/°C at 22 °C |
| $d$ | = | Displacement, m |
| $F_G$ | = | fiber Bragg grating gage factor, 0.796 at 22 °C |
| $N_C$ | = | condition number |
| $R$ | = | cross-correlation function |
| $S$ | = | strain conversion matrix, $\mu$m/m |
| $[T_{\mathrm{ds}}]$ | = | displacement-strain transformation matrix, $\mathrm{m}^2/\mu$m |
| $n_e$ | = | effective refractive index of the fiber core |
| $\Delta T$ | = | temperature change, °C |
| $\Delta\lambda$ | = | fiber Bragg grating wavelength shift, nm |
| $\varepsilon$ | = | strain, $\mu$m/m |
| $\varepsilon_{\mathrm{TO}}$ | = | thermally induced apparent strain, $\mu$m/m |
| $\eta$ | = | generalized coordinate |
| $\lambda_0$ | = | fiber Bragg grating nominal wavelength, nm |
| $\lambda_B$ | = | Bragg wavelength of the fiber Bragg grating sensor array, nm |
| $\Lambda$ | = | grating period, $\mathrm{m}^{-1}$ |
| $\Phi$ | = | displacement mode shape, m |
| $\Psi$ | = | strain mode shape, $\mu$m/m |

## I. Introduction

MISSILES and launch vehicles are typically slender in shape to reduce aerodynamic drag [1]. To stabilize the trajectory of a rocket while considering its flexible dynamics, the estimation of modal frequencies and modal shapes is a critical aspect of mission planning and controller design. Because the system's mass changes in time because of propellant expenditure, modal characteristics also change with time. In [2], Tobbe et al. describe a typical estimation method for the variation of modal properties during flight based on interpolation from precalculated look-up tables of both modal frequencies and modal shapes. Based on this kind of off-line interpolation approach, several adaptive methods have been applied to rocket flight control, as described in [3–7]. Notch filter solutions exist that isolate the source of vibrations from the controller. A downside of the notch filter technique is given by the addition of a phase lag to the control system that yields a reduction of phase margin up to loss of stability [8]. Although in heavy lift vehicles the estimation of flexible dynamics has not been a critical factor, this is bound to change as more slender and lighter vehicles are considered.

Current literature describes the use of strain gages and piezoelectric sensors [9,10] as the standard approach for deflection monitoring and modal shape identification of launch vehicles. Although the use of additional onboard instrumentation would provide more accurate estimation of modal properties, which is better suited for real-time control, increasing the quality of the estimation requires an increasingly large number of sensors, and the weight and complexity quickly become prohibitive. Furthermore, the extensive wiring required is not only heavy but also susceptible to electromagnetic interference.

Fiber Bragg grating (FBG) sensors [11–14] open the possibility of measurement of strain and estimation of shapes and modal properties of aerospace structures in real time. FBG sensors have multiple advantages, being small, lightweight, immune to electromagnetic interference, and installable in large numbers with relatively small weight penalties. With state of the art interrogation equipment, the sampling rate of FBG sensors can be as high as 2500 Hz (buffered) and up to 1000 Hz nonmultiplexed unbuffered. This presents possibilities to use strain data in multiple points on a structure to estimate modal shapes in real time.

One of the important mathematical properties of quasi-static modal properties is that the mean of the cross correlation of any pair of different modal shapes is zero [15,16], which geometrically means that the modal coordinates of any two different modal shapes are orthogonal vectors. Based on this property, modal shapes can be reconstructed in real time from a finite number of strain measurements in the structure. Mathematically it can be shown that only $n$ FBG sensors are needed to estimate up to $n$ modal shapes, although in practice better estimation is achieved with a number of sensors larger than the number of modes to be estimated.

Received 27 October 2011; revision received 2 July 2012; accepted for publication 2 July 2012; published online 22 November 2012. Copyright © 2012 by the American Institute of Aeronautics and Astronautics, Inc. All rights reserved. Copies of this paper may be made for personal or internal use, on condition that the copier pay the $10.00 per-copy fee to the Copyright Clearance Center, Inc., 222 Rosewood Drive, Danvers, MA 01923; include the code 1533-385X/12 and $10.00 in correspondence with the CCC.

*Ph.D. Candidate, Department of Mechanical and Aerospace Engineering. Student Member AIAA.

†Ph.D. Candidate, Department of Electrical and Computer Engineering. Student Member AIAA.

‡Associate Professor, Department of Mechanical and Aerospace Engineering. Associate Fellow AIAA.

§Associate Professor, Department of Mechanical and Aerospace Engineering.

Downloaded by STANFORD UNIVERSITY on March 24, 2013 | http://arc.aiaa.org | DOI: 10.2514/1.J051702

This paper is organized as follows. The basic theory and algorithms for modal shape reconstruction using FBG sensors are introduced in Sec. II. In Sec. III, the proposed modal shape reconstruction method is applied to analyze the bending vibration of an ideal cantilever beam, and the results are compared with modal shapes obtained from numerical calculations for an ideal beam. Section IV presents experimental validation of the proposed method by providing real-time modal shape estimation when the system is subject to a step change in mass. Conclusions are drawn in Sec. V.

## II. Theory and Method

This section presents the basic theory and algorithms for real-time modal shape reconstruction using FBG sensors of a mass varying system in real time.

### A. Measurement of Strain Using FBG Sensors

A FBG sensor consists of localized periodic changes of the refractive index at the core of an optical fiber, generated by exposure to an intense ultraviolet laser interference pattern at a specified nominal wavelength. If broadband light is injected into an optical fiber carrying a FBG sensor, a specific wavelength component is reflected, which is the Bragg wavelength. The Bragg condition is expressed in Eq. (1):

$$\lambda_B = 2n_e\Lambda \tag{1}$$

where $\lambda_B$ is the Bragg wavelength of the FBG sensor, $n_e$ is the effective refractive index of the fiber core, and $\Lambda$ is the grating period. The wavelength given by the Bragg condition is reflected by the grating, whereas other wavelengths pass through with minimal attenuation, as shown in Fig. 1.

By measuring the intensity change in the reflected wavelength at a specific FBG sensor within a fiber, the change in a physical property at the sensor location (such as either strain or temperature) can be measured. The shift of the Bragg wavelength caused by strain and temperature are shown in Eqs. (2) and (3). Equation (2) calculates strain from the wavelength shift $\Delta\lambda$, where $\varepsilon_{\mathrm{TO}}$ is the strain caused by temperature changes:

$$\varepsilon = \left(\frac{\Delta\lambda}{\lambda_0}\right)\frac{1\times 10^6}{F_G} - \varepsilon_{\mathrm{TO}} \tag{2}$$

$$\varepsilon_{\mathrm{TO}} = \Delta T\left[\frac{C_1}{F_G} + \mathrm{CTE}_s - C_2\right] \tag{3}$$

$C_1$, $F_G$, $\mathrm{CTE}_s$, and $C_2$ in Eq. (3) are constants and are the same for all FBG sensors within a fiber; they are used to compensate strain measurements for temperature changes. To implement temperature compensation, one FBG sensor is mounted at a point on the test specimen that does not experience any strain. The wavelength shift measured by this sensor can be entirely attributed to temperature change and is equal to $-\varepsilon_{\mathrm{TO}}$. The other FBG strain measurements are then compensated for temperature change by subtracting this result from their corresponding measurement.

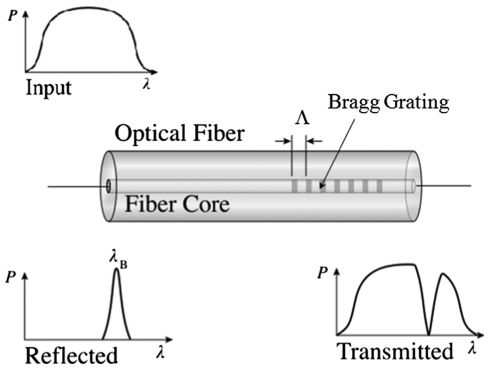


**Fig. 1 Fiber Bragg Grating structure with refractive index profile and spectral response.**

### B. FBG Array Configuration

The displacement of individual points on a test specimen can be expressed in terms of the summation of the contributions of a finite number of vibration modes and can be related to measured strains through a strain-displacement relationship. By placing multiple strain sensors on a test article, multiple modes can be taken into account to achieve suitable precision in the estimation of deflection. To optimize the estimation, sensor locations are selected such that the transformation matrix has the smallest possible condition number [17]. Theoretically, $n$ modes can be estimated by $n$ sensors, but in practice the number of sensors and the sensors' location significantly affect the accuracy of the estimation. Dyllong and Kreuder [18] presented a method to find the optimized number and placement of strain sensors for modal estimation and quantified the accuracy in the estimation of the first three modes using five sensors based on spline interpolation.

The displacement-strain transformation matrix $[T_{\mathrm{ds}}]$ can be expressed in terms of the strain modal shape matrix $[\Psi]$ and the displacement modal shape matrix $[\Phi]$ as shown in Eq. (4):

$$[T_{\mathrm{ds}}]_{n\times M} = [\Phi]_{n\times N}([\Psi]^T_{N\times M}[\Psi]_{M\times N})^{-1}[\Psi]^T_{N\times M} \tag{4}$$

where $M$ is the number of sensors, $N$ is the number of mode shapes considered, and $n$ is the number of beam elements whose deflection is being estimated. The condition number $N_C$ of the displacement-strain transformation matrix $[T_{\mathrm{ds}}]$ can be interpreted as the upper bound of the displacement error relative to the change in strain measurement [12,19]. The condition number defined in Eq. (5) can be used as a quality metric of the displacement-strain transformation matrix. Sensor location can be optimized by choosing the sensor arrangement that minimizes$N_C$. A smaller $N_C$ yields more accurate shape estimation:

$$N_C = \|[T_{\mathrm{ds}}]\| \bullet \|[T_{\mathrm{ds}}]^{-1}\| \tag{5}$$

where the operator $\|\bullet\|$ denotes the Euclidean norm of the matrix.

### C. Experimental Test Platform

Modeling a rocket as a flexible beam is a widely accepted representation of the launch vehicle's flexible dynamics [1–8]. A vertical rectangular cantilever aluminum beam as shown in Fig. 2 was used in the validation experiments, where beam width is 25.4 mm and beam thickness is 3.175 mm. The base of the vertical beam is mounted to a linear motor stage that can excite the beam with a computer-controlled signal. The linear motor is driven by an Aerotech BA series linear servo amplifier, controlled using a real-time target computer (xPC target, from SpeedGoat, GmbH). The position of

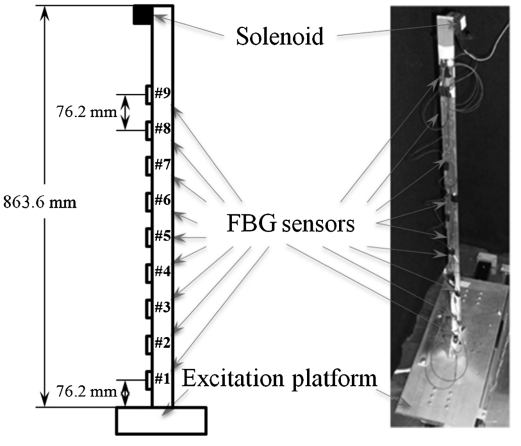


**Fig. 2 FBG sensor array configuration and test platform.**

the moving base is controlled by a proportional-integral-derivative (PID) feedback loop, and the position of the stage is measured using a Novotechnik TLH 360 position transducer.

A FBG sensor array consisting of nine sensors was installed on the beam. The sensors are attached with epoxy on one side of the beam. Equally spaced sensor locations were selected because this configuration gave the smallest condition number within the various configurations considered. An extra sensor is installed on the stage to compensate for the temperature and environment disturbances. To estimate time-varying modal shapes, a step change in mass was introduced by releasing a solenoid core attached to the free end of the beam: separation could be enabled when a digital control pulse was sent to the coil's power supply. Detaching the solenoid changes the mass of the beam assembly, changing its modal shapes. The beam's support is attached to a platform mounted on air bearings and driven by two linear motors that can be used to create arbitrary base excitation in the beam up to 60 Hz.

Two cases are examined. First, the strain mode shapes of the beam without the solenoid are compared with finite element results of an ideal cantilever beam. Second, the solenoid is used to introduce a step change in mass at a specified time during the experiment. The change in modal shapes and the convergence of the estimation are examined in the second case.

### D. Estimation of Mode Shapes

The displacement and strain of structures can be expressed using a finite number of mode shapes, $N$. The strain and displacement at any point in the beam $x$ at any time $t$ can be represented by the summation of their mode shapes weighed by the corresponding generalized coordinates:

$$d(x, y, z, t) = \sum_{i=1}^{N} \Phi_i(x, y, z)\eta_i(t) \tag{6}$$

$$\varepsilon(x, y, z, t) = \sum_{i=1}^{N} \Psi_i(x, y, z)\eta_i(t) \tag{7}$$

where $d$ and $\varepsilon$ are the corresponding displacement and strain functions of the entire beam $(x, y, z)$ at time $t$. $\Phi_i$ and $\eta_i$ are the $i$th deflection modal shape and $i$th strain modal shape, respectively, and $\eta_i$ is the corresponding $i$th generalized coordinate, where $N$ is the highest order mode being considered.

Suppose there is a strain weight matrix $S$ whose entries $S_{ij}$ can be used to estimate the $i$th generalized coordinate based on $M$ measurements of strain as shown in Eq. (8):

$$\hat{\eta}_i(t) = \sum_{j=1}^{M} S_{ij}\varepsilon_j(t) \tag{8}$$

where $\varepsilon_j(t)$ is the strain measured by the $j$th sensor in time, $j$ going from 1 to $M$, and $S_{ij}$ is the weight for the $j$th sensor on the $i$th mode. For all $N$ modes being considered based on $M$ sensors, Eq. (8) can be written in matrix form as

$$\hat{\eta}_{(N\times 1)} = S_{(N\times M)}\varepsilon_{(M\times 1)} \tag{9}$$

Using beam theory, strain-displacement relation can be obtained as shown in [17]:

$$\varepsilon(x, t) = -\frac{h}{2}\frac{\partial^2 d(x, t)}{\partial x^2} = -\frac{h}{2}\sum_{i=1}^{N} \Phi_i''(x)\eta_i(t) \tag{10}$$

The matrix form of Eq. (10) can be combined with Eq. (7) to yield

$$\varepsilon_{M\times 1} = C_{M\times N}\eta_{N\times 1} = \Psi_{M\times N}\eta_{N\times 1} \tag{11}$$

where $C(j, i) = -\frac{h}{2}\Phi_i''(x_j)$ and $\Phi_i''(x_j)$ is the second spatial derivative of the $i$th mode shape at position $x_j$. Combining Eq. (11) and Eq. (9):

$$\hat{\eta}_{N\times 1} = S_{N\times M}C_{M\times N}\eta_{N\times 1} \tag{12}$$

Because $\hat{\eta} \approx \eta$, $S$ should be equal to $C^{-1}$. If $C^{-1}$ exists, then $C$ must be square and $M = N$, which means at least $N$ sensors are needed to estimate $N$ modes. When the number of sensors is more than $N$, the strain mode shape can be obtained as

$$\Psi_{M\times N} = ([S]_{M\times N}^T[S]_{N\times M})^{-1}[S]_{M\times N}^T \tag{13}$$

The strain weight matrix defined here is very similar to the modal filter coefficients used in modal control [20]. If the exact loading conditions applied on the structure are known, the matrix can be obtained by solving the equation of motion

$$\eta_i + 2\zeta_i\Omega_i\dot{\eta}_i + \Omega_i^2\eta_i = \frac{Q_i}{M_i} \tag{14}$$

where the generalized mass is $M_i = \int_0^L m\Phi_i^2\,\mathrm{d}l$ and the generalized force is $Q_i = \int_0^L \sum F_l\Phi_i\,\mathrm{d}l$. $\zeta_i$ is the $i$th mode damping factor, $\Omega_i$ is the $i$th mode frequency, $\Phi_i$ is the $i$th mode shape, $m$ is the mass per unit length, $L$ is the rocket length, and $F_l$ is the force per unit length.

Because the real-time loading conditions of a rocket during flight are very difficult to predict, it is necessary to find an alternate way to estimate the strain weight matrix. Sumali [21] suggested using the correlation matrix to reduce the knowledge of necessary constraint conditions and estimated the displacement mode shapes of a fixed-fixed end ideal uniform beam by using the voltage readings of the continuous distributed piezoelectric polyvinylidene fluoride film sensors.

### E. Estimation of $S$ via Cross-Correlation Function

The cross correlation of two different modes with zero lag is defined as

$$R_{ij} = E[\eta_i(k)\eta_j(k)] = \frac{1}{k}\lim_{k\to\infty}\sum_{t=1}^{k}\eta_i(t)\eta_j(t) \tag{15}$$

If $\eta_i(t)$ and $\eta_j(t)$ are generalized coordinates, they must be orthogonal to each other:

$$\lim_{k\to\infty} R_{ij}(k) = 0; \qquad i \neq j \tag{16}$$

Equation (16) also means the matrix $R$ should be diagonal. This property of the cross-correlation function of generalized coordinates can be illustrated by simulation of a simple cantilever beam as shown in Fig. 3. The cross correlation of the first and third modes obtained by Eq. (15) converges to zero.

Replacing the estimated generalized coordinates [Eq. (9)] in the condition given by Eq. (15) yields

$$R = E[\hat{\eta}_i(k)\hat{\eta}_j(k)] = E[S\varepsilon\varepsilon^T S^T] = SE[\varepsilon\varepsilon^T]S^T \tag{17}$$

In Eq. (17) $R$ should be a diagonal matrix, and $E[\varepsilon\varepsilon^T]$ is diagonalizable with an eigenvector matrix $P$, where $P_m$ is the $m$th eigenvector of $E[\varepsilon\varepsilon^T]$. This means that$P^{-1}E[\varepsilon\varepsilon^T]P$ is diagonal, and therefore $P^{-1} = P^T$. Without loss of generality, $S = P^T$ can be used to diagonalize $R$; thus the strain-weight matrix $S$ can be obtained by finding the eigenvectors of $E[\varepsilon\varepsilon^T]$. With the strain-weight matrix $S$, the strain mode shapes can be calculated according to Eq. (13). Thus, the estimation of strain mode shapes is reduced to finding the normalized eigenvectors of the mean cross-correlation matrix of strain.

### F. Spatial Integration of Strain Mode Shape

The relationship between strain mode shapes and displacement mode shapes is shown in Eq. (10). Displacement mode shapes can be obtained by taking two successive spatial integrations of the strain mode shapes. When the mode shapes at several locations are needed,

Downloaded by STANFORD UNIVERSITY on March 24, 2013 | http://arc.aiaa.org | DOI: 10.2514/1.J051702

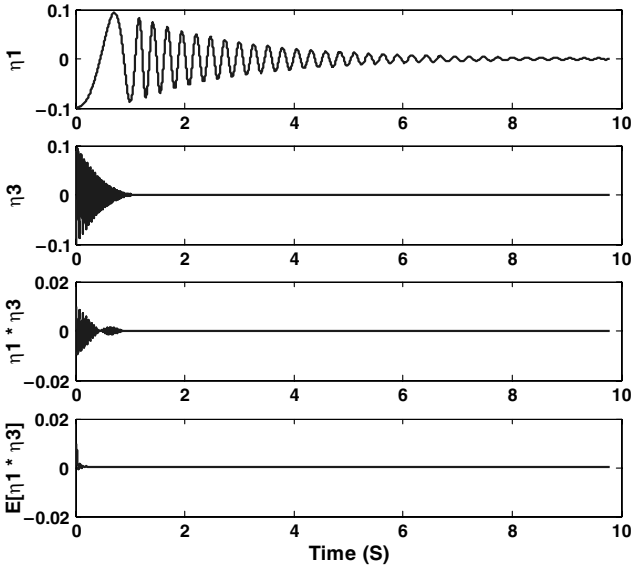


**Fig. 3 The first and third generalized coordinates and their cross-correlation function.**

more sensors or spline interpolation can be used to reduce the numerical errors introduced by the integration. The performance of direct spatial integration based on 9-sensor array and 34-sensor array can be depicted by Figs. 4 and 5, respectively. To reduce the numerical error introduced by the integration, spline interpolation can be used. In the beam shown in Fig. 2, the strain and displacement mode shapes are calculated analytically. Nine and thirty-four points of strain mode shapes are sampled for each mode for comparison purposes. We used spline interpolation to expand the representation of each mode to 341 points. Trapezoidal integration is applied on the expanded mode shapes twice, and the displacement mode shapes are obtained and truncated back to 9 and 34 points.

As shown in Fig. 4, the first two displacement mode shapes can be found adequately. The estimation of the third mode is degraded by the numerical errors. If 34 sensors can be used on the beam, the results shown in Fig. 5 are significantly improved. The results show the higher-mode estimations are more sensitive to the number of sensors. Additionally, the convergence of the estimation accuracy demonstrates the feasibility of the displacement mode shapes being obtained by strain mode shapes mathematically. Because the strain mode shapes, displacement mode shapes, and the strain data are known, the deflection can be estimated at any point in the test article based on strain to displacement transform matrix given in Eq. (4).

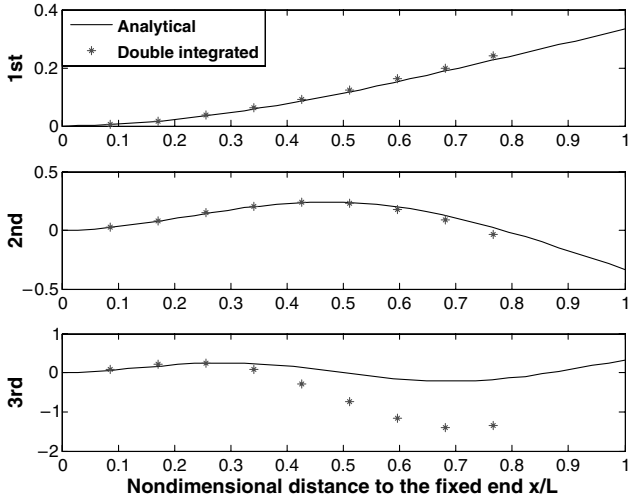


**Fig. 4 Displacement mode shapes obtained by interpolation and integration based nine-sensor array.**

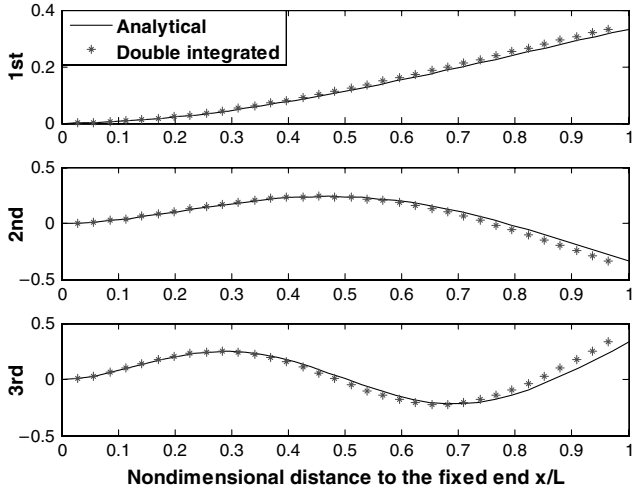


**Fig. 5 Displacement mode shapes obtained by interpolation and integration based 34-sensor array.**

### G. Algorithm

To estimate the time-varying mode shapes in real time, the estimation of the strain weight matrix should be done in real time. We adopt the method based on a sliding window to calculate the real-time updated cross-correlation matrix. According to the theory and equations given in Sec. II.D, the mode shape estimations will be updated in real time by calculating the eigenvectors of the cross-correlation matrix in each cycle. The algorithm can be summarized by Table 1. The minimum size of the sliding window depends on the convergence of the cross-correlation function. As shown in Fig. 3, the cross-correlation function converges in a limited number of time samples, which implies that "real-time" estimation is possible.

Based on the algorithm given in Table 1, the mode shape estimation can be updated at every time sample. Thus, the real-time modal information is extracted from the strain history using a rolling window, capturing the mode shape changes in time. In the next two sections, simulation and experiments are used to demonstrate the validity and numerical efficiency of the proposed method.

## III. Simulation Results

To assess the feasibility of the proposed method for mode shape reconstruction, strain values in the test specimen were estimated from analytical solutions of strain mode shapes for a simple cantilever beam. The corresponding beam vibration was simulated by Matlab/Simulink using a finite number of discrete beam elements. The first six strain mode shapes were estimated based on 500 samples of sensor outputs without using any information on structure and excitation. Uniformly distributed sensor configurations of 9, 30, and 50 sensors are considered in the simulation. The first three strain and displacement mode shapes were estimated and compared with the theoretical values; the comparisons are shown in Figs. 6 and 7, respectively. The vertical axis values are obtained by normalizing strain/displacement by the number of points in the strain/displacement vector.

As shown in both Figs. 6 and 7, the estimation error increases in higher-order modes. For the first mode estimation, a nine-sensor array gives a good estimation on mode shape. For the second mode and third mode estimations, the estimation error of the nine-sensor array increased. The numerical error affects not only the magnitude of each component but also the peak locations of the shape curvature, especially for estimation of higher order modes. This is because nine sensors are not enough to accurately capture the peak locations of a complex spatial curve such as the third mode. When the number of sensor is higher than 30, mode shape estimations are very close to the theoretical values. The results shown in Figs. 6 and 7 suggest that the estimation converges to the theoretical value with increasing sensor count. The estimation error can be defined as:

Downloaded by STANFORD UNIVERSITY on March 24, 2013 | http://arc.aiaa.org | DOI: 10.2514/1.J051702

**Table 1 Algorithm summary**

Step 1: Define the size of the sliding window $K$.
Step 2: Calculate the cross-correlation function $R$ at time $t$ based on the strain measured from $t - K + 1$ to $t$.
If ($t <= K$)
$R(t) = \text{strain}(t)^{*}\text{strain}(t)' + (t-1)^{*}R(t-1)/t$;
else
$R(t) = \text{strain}(t)^{*}\text{strain}(t)' + (K-1)^{*}(R(t-1) - R(t-K))/K$;
Step 3: Calculate the eigenvectors of matrix $R$ to find the strain mode shapes:
$[u, l] = \text{eig}(R)$;
Step 4: Calculate the displacement mode shapes.
Using spatial spline interpolation and numerical integration, the displacement mode shapes can be found.

$$\text{error}_i = \frac{1}{M}\sqrt{\sum_{j=1}^{M}\left(\frac{\text{error}_{ij}}{\Phi_{ij}}\right)^2} \tag{18}$$

where $\text{error}_i$ is the error on the estimation of the $i$th mode, $\text{error}_{ij}$ is the error at each node ($i$th mode, $j$th node), and $M$ is the total number of the sensors (which in this case equals the number of nodes). The total strain and displacement estimation errors for each mode are shown in Table 2.

FBG sensor arrays allow accurate strain to displacement conversion provided that a good estimate of the displacement mode shapes (e.g., from a FEM analysis) is available. An excitation force was applied on the beam for 1.5 s, and the beam continues free vibration. Using the strain-displacement transform matrix, the displacements calculated from the FBG strain measurements are in excellent agreement with the displacement outputs of the analytical beam model, as shown in Fig. 8.

A set of simulations were examined with different mode shape settings and initial conditions. The results show that the proposed mode shape estimation method has consistent performance and can be used to estimate the mode shapes of a structure with time varying properties.

## IV. Experimental Validation

In this section, the proposed method for on-line mode shape estimation is validated by experiments on a vertical cantilever beam by providing real-time modal shape estimation when the system is subject to a step change in mass.

### A. Experimental Results: Beam with Constant Mass

For a uniform beam, the analytical expression for displacement mode shapes is:

$$\Phi_i(x) = \sin\beta_i x - \sinh\beta_i x - \frac{\sin\beta_i L + \sinh\beta_i L}{\cos\beta_i L + \cosh\beta_i L}(\cos\beta_i x - \cosh\beta_i x) \tag{19}$$

The strain mode shapes for each mode are

$$\Psi_i(x) = \frac{\mathrm{d}^2\Phi_i(x)}{\mathrm{d}x^2} = -\beta_i^2\sin\beta_i x - \beta_i^2\sinh\beta_i x - \frac{\sin\beta_i L + \sinh\beta_i L}{\cos\beta_i L + \cosh\beta_i L}(-\beta_i^2\cos\beta_i x - \beta_i^2\cosh\beta_i x) \tag{20}$$

where $\cos\beta_i L\cosh\beta_i L = -1$. From properties of trigonometric and hyperbolic functions, a relationship between strain and displacement mode shapes can be shown to be:

$$\Phi_i(L - x) = (-1)^{i-1}\text{Const}_i\Psi_i(x) \tag{21}$$

That is, in the ideal uniform beam example, the displacement mode shapes can be calculated from the displacement mode shapes without using double integration of strain using Eq. (20). If the beam is not ideal, numerical integration must be used to calculate the displacement mode shapes from strain measurements.

Using the test platform described in Sec. II, the strain and displacement mode shapes obtained based on Eqs. (18) and (19) are compared with those estimated using nine sampling points on a numerically simulated beam in Matlab/Simulink and with those estimated from measurements of a FBG sensor array (consisting of nine sensors). As shown in Figs. 9 and 10, the presented method can give adequate estimation of strain and displacement mode shapes.

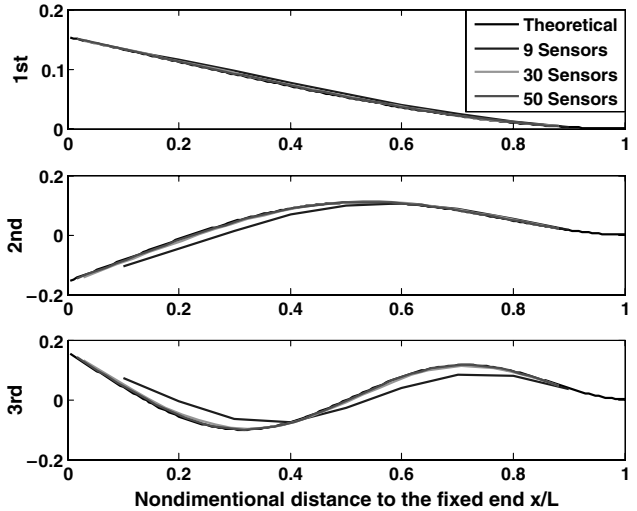


**Fig. 6 First three strain modal shape estimated results with different numbers of sensors.**

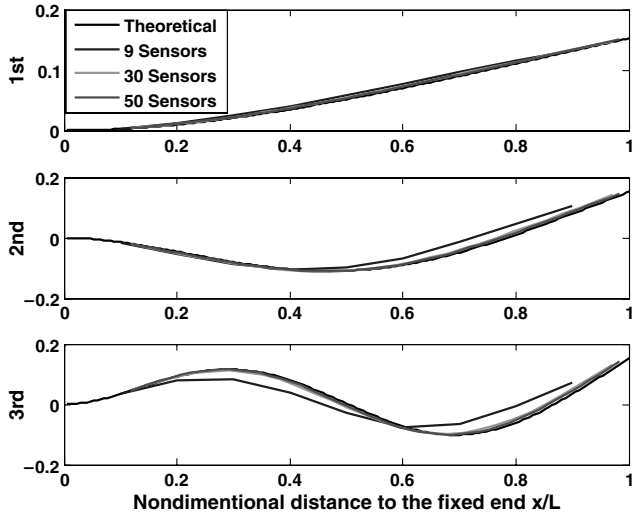


**Fig. 7 First three displacement mode shapes estimated with different numbers of sensors.**

Downloaded by STANFORD UNIVERSITY on March 24, 2013 | http://arc.aiaa.org | DOI: 10.2514/1.J051702

**Table 2 Strain mode shapes estimation error (sum of squared errors) based on different sensor counts**

| | First mode | Second mode | Third mode | Fourth mode | Fifth mode | Sixth mode |
|---|---|---|---|---|---|---|
| 9 Sensors | 0.0032 | 0.0267 | 0.0442 | 0.0606 | 0.0809 | 0.1136 |
| 30 Sensors | 0.0002 | 0.0016 | 0.0019 | 0.0021 | 0.0024 | 0.0048 |
| 50 Sensors | 0.00006 | 0.00035 | 0.0005 | 0.0011 | 0.0023 | 0.0038 |

The first mode shapes estimated based on both numerical simulation and real FBG measurements are almost identical to the theoretical values [sum of squared error (SS error) equal to 0.0148]. For the second and third mode, the error is increased because of the limitation in the number of sensors. The numerical and Fiber Optics Sensor (FOS) mode shape traces shown in Fig. 10 are calculated based on Eq. (20).

### B. Experimental Results: Modal Estimation During a Step Change in Mass

A 100-g solenoid was temporarily attached to the free end of the beam via a small iron plunger (10 g) glued to the test article. When excitation to the solenoid coil is interrupted, the solenoid detaches from the plunger, introducing a step change in mass of the beam. An 800-point rolling buffer of strain measurements was used to estimate the first two strain mode shapes, after which the calculated strain mode shapes are updated every millisecond (the strain transducer can be interrogated up to 1000 Hz). The first and second strain mode shapes were estimated from time domain data from an array of nine FBG sensors. The corresponding mode shapes of the beam with sensors installed, before and after the step change in mass occurs, are shown in Fig. 11. The mode shapes obtained in Fig. 11 are normalized to a unit vector for convenience of comparison. The changes in strain mode shapes are captured.

To demonstrate the accuracy of the proposed method for on-line mode shape estimation, the time-varying mode shapes estimated using the FBG array were compared with theoretical values obtained in ANSYS. For the comparison and without losing generality, the mode shapes obtained were normalized. Because the first sensor

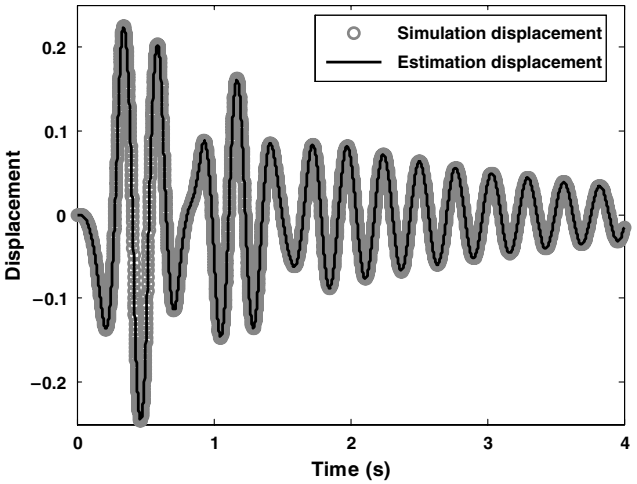


**Fig. 8 Estimated and actual displacement of the free end of a cantilever beam.**

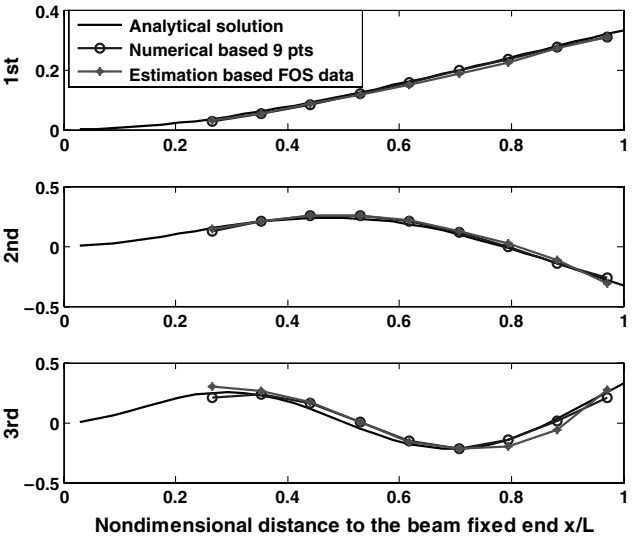


**Fig. 10 Estimated displacement mode shapes of the first three modes of the test article.**

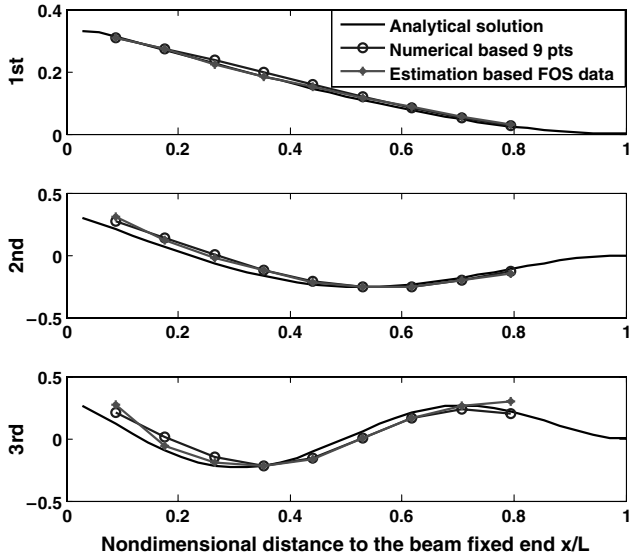


**Fig. 9 Estimated strain mode shapes of the first three modes of the test article.**

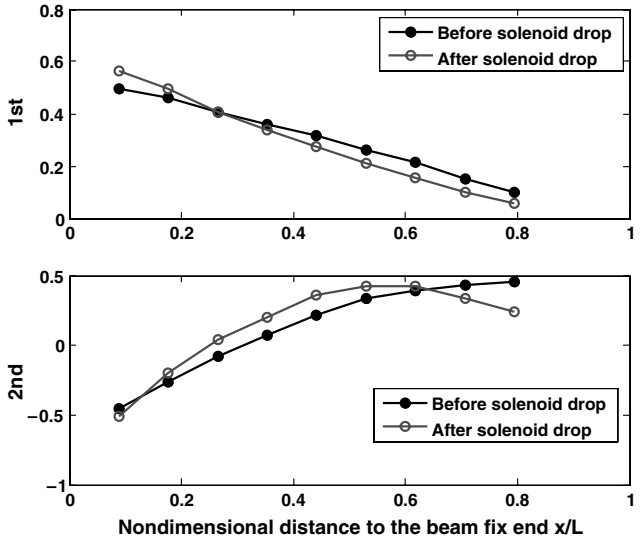


**Fig. 11 Change in first two mode shapes before and after solenoid mass drop.**

Downloaded by STANFORD UNIVERSITY on March 24, 2013 | http://arc.aiaa.org | DOI: 10.2514/1.J051702

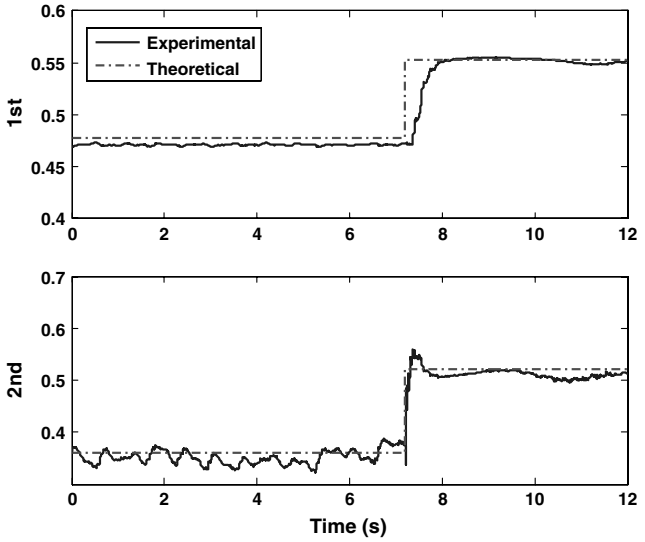


**Fig. 12 Change in the first two strain mode shape components at the first sensor location.**

(near the fixed end of the beam) has the largest strain, the strain mode shape component at this point was used for scaling. The change in time of the first two mode shapes at the first sensor is shown in Fig. 12.

As shown in Fig. 12, the first mode shape estimation took about 0.8 s to approach the theoretical mode shape after the solenoid dropped. The 0.8-s lag corresponds to the 800-point rolling buffer at a 1 kHz sampling rate. The estimation of the change in the second mode is much faster than that of the first mode because of its higher frequency. The small fluctuation in second mode estimation suggests that more sensors are needed to achieve more accurate estimations of higher modes. The proposed method can detect the real-time mode shapes changes without having to make any assumptions on the exact constraint conditions.

## V. Conclusions

A method to estimate mode shapes of a structure that vibrates in one plane, based on an array of strain measurements in real time has been presented. The method uses the cross-correlation properties of different modes to define the transformation matrix that allows estimation of the generalized coordinate functions for a given time history of the vector of strain in $M$ locations. With the FBG sensor array consisting of nine sensors, the mode shape estimation errors of the first three modes are 0.3, 2.7, and 4.4%, respectively. The estimation results converge to the theoretical values with an increasing in the number of strain sensors. Comparisons with both analytical results and experiments validate the proposed method. With a 1000-Hz sampling rate, the results show that both strain and displacement mode shapes can be obtained from strain data within 0.5–0.8 s without other information about the specimen such as geometry or material properties or previous knowledge of natural frequencies. The proposed approach is well suited to estimate changes in modal shapes in real time caused by dynamic changes in mass, as needed for real-time control of flexible launch vehicles. Fiber Bragg sensors also enable real-time monitoring of deflections in a structure via the displacement-strain transformation of a strain vector measured by an FBG array.

Natural frequencies and mode shapes are generally not defined in structures with continuous time-varying mass properties such as a rocket. However, if the sampling rate of an array of strain sensors is fast compared with the rate of change of mass (a modern FBG interrogator can be sampled at rates in excess of 2000 Hz), modal properties can be defined in a semistatic sense: the mass change is semistationary relative to the speed at which the mode shapes can be estimated. The mass change of a rocket can be regarded as the result of many small step changes in mass. If the changes in mode shapes can be estimated with a small number of time samples, the present method can be used to assess mode shape changes in real time.

In the example shown, the effect of an abrupt mass change (such as a separation event) in the modal properties of the structure can be successfully detected. This is of particular interest for launch vehicle concepts where vibration damping after separation is critical.

## Acknowledgments

This work was partly supported by NASA-Analex under Agreement No. 10-013. The authors want to thank Michael Wolf, James Stanley, and Jon Bauschlicher from NASA-KSC Launch Services Program for their support and feedback.

## References

[1] Gregory, I. M., "Stability Result for Dynamic Inversion Devised to Control Large Flexible Aircraft," *AIAA Guidance, Navigation, and Control Conference*, AIAA Paper 2001-4284, Montreal, Quebec, Canada, Aug. 6–9, 2001, pp. 1–13.

[2] Tobbe, P. A., Matras, A. L., and Wilson, H. E., "Modeling and Simulation of Variable Mass, Flexible Structures," *AIAA Modeling and Simulation Technologies Conference*, AIAA Paper 2009-6023, Chicago, IL, 2009.

[3] Choi, H., and Bang, H., "An Adaptive Control Approach to the Attitude Control of a Flexible Rocket," *Control Engineering Practice*, Vol. 8, No. 9, 2000, pp. 1003–1010. doi:10.1016/S0967-0661(00)00032-0

[4] Choi, H., and Jim, J., "Adaptive Notch Filter Design for Bending Vibration of a Sounding Rocket," *Proceedings of the Institution of Mechanical Engineers–Part G*, Vol. 215, No. 1, 2001, pp. 13–23. doi:10.1243/0954410011531718

[5] Khoshnood, A., Roshanian, J., and Khaki-Sedig, A., "Model Reference Adaptive Control for a Flexible Launch Vehicle," *Proceedings of the Institution of Mechanical Engineers–Part I: Journal of Systems and Control Engineering*, Vol. 222, No. 1, 2008, pp. 49–55. doi:10.1243/09596518JSCE469.

[6] Khoshnood, A., Roshanian, J., Jafari, A., and Khaki-Sedig, A., "Simultaneous Estimation of Two Bending Vibration Frequencies for Attitude Control of a Flexible Launch Vehicle," *Proceedings of the Institution of Mechanical Engineers–Part I: Journal of Systems and Control Engineering*, Vol. 223, No. 5, 2009, pp. 721–726. doi:10.1243/09596518JSCE769

[7] Kharisov, E., Gregory, I., Cao, C., and Hovakimyan, N., "L1 Adaptive Control Law for Flexible Space Launch Vehicle and Proposed Plan for Flight Test Validation," *AIAA Guidance, Navigation and Control Conference and Exhibit*, AIAA Paper 2008-7128, Honolulu, HI, Aug. 18–21, 2008.

[8] Shtessel, Y., and Baev, S., "Active Compensation of Low Frequency Flexible Modes of Crew Launch Vehicle Using Sliding Mode Observers," *AIAA Guidance, Navigation and Control Conference and Exhibit*, AIAA Paper 2008-7127, Honolulu, HI, Aug. 18–21, 2008.

[9] Sunar, M., and Al-Bedoor, B., "Vibration Measurement of a Cantilever Beam Using Root Embedded Piezoceramic Sensor," *Proceedings of the Institution of Mechanical Engineers–Part C: Journal of Mechanical Engineering Science*, Vol. 222, No. 2, 2008, pp. 147–161. doi:10.1243/09544062JMES621

[10] Kon, S., Oldham, K., and Horowitz, R., "Piezoresistive and Piezoelectric MEMS Strain Sensors for Vibration Detection," *Proceedings of SPIE*, Vol. 6529, April 2007, pp. 1–11, 65292V. doi:10.1117/12.715814

[11] Rapp, S., Kang, L., Mueller, U., Han, J., and Baier, H., "Dynamic Shape Estimation by Modal Approach Using Fiber Bragg Grating Strain Sensors," *Proceedings of SPIE*, Vol. 6529, 2007, pp. 1–11, 65293E. doi:10.1117/12.715634

[12] Kang, L.-H., Kim, D.-K., and Han, J.-H., "Estimation of Dynamic Structural Displacements Using Fiber Bragg Grating Strain Sensors," *Journal of Sound and Vibration*, Vol. 305, No. 3, 2007, pp. 534–542. doi:10.1016/j.jsv.2007.04.037

[13] Richards, W. L., "Fiber Optic Wing Shape Sensing on the IKHANA Vehicle," NASA Rept. 20070031051, 2007.

[14] Kim, H.-I., Kang, L.-H., and Han, J.-H., "Shape Estimation with Distributed Fiber Bragg Grating Sensors for Rotating Structures," *Smart Materials and Structures*, Vol. 20, No. 3, 2011, p. 0035011. doi:10.1088/0964-1726/20/3/035011

[15] Craig, R. R., and Kurdila, A. J., *Fundamentals of Structural and Dynamics*, 2nd ed., John Wiley & Sons, Inc., Hoboken, NJ, 2006, pp. 10, 281–324.

Downloaded by STANFORD UNIVERSITY on March 24, 2013 | http://arc.aiaa.org | DOI: 10.2514/1.J051702

[16] Kelly, S. G., *Fundamentals of Mechanical Vibrations*, 2nd ed., McGraw-Hill Higher Education, New York, 2000, pp. 6, 325.
[17] Li, C.-J., and Ulsoy, A.G., "High-Precision Measurement of Tool-Tip Displacement Using Strain Gauges in Precision Flexible Line Boring," *Mechanical Systems and Signal Processing*, Vol. 13, 1999, pp. 531–546.
doi:10.1006/mssp.1999.1223
[18] Dyllong, E., and Kreuder, A., "Optimal Reconstruction of Mode Shapes Using Non-Uniform Strain Sensor Spacing," *Proceeding of the 1999 IEEE/ASME International Conference on Advanced Intelligent Mechatronics*, Atlanta, GA, Sept. 19–23, 1999, pp. 150–155.
[19] Rapp, S., Kang, L.-H., Han, J.-H., Mueller, U., and Baier, H., "Displacement Field Estimation for a Two-Dimensional Structure Using Fiber Bragg Grating Sensors," *Smart Materials and Structures*, Vol. 18, No. 2, 2009, p. 0225006.
doi:10.1088/0964-1726/18/2/025006
[20] Meirovitch, L., and Baruh, H., "Control of Self-Adjoint Distributed-Parameter Systems," *AIAA Journal of Guidance, Control and Dynamics*, Vol. 5, No. 1, 1982, pp. 60–66.
doi:10.2514/3.56140
[21] Sumali, H., "A New Adapative Array of Vibration Sensors," Ph.D. Dissertation, Mechanical Engineering Dept., Virginia Tech., Blacksburg, VA, 1997.

N. Wereley
*Associate Editor*

Downloaded by STANFORD UNIVERSITY on March 24, 2013 | http://arc.aiaa.org | DOI: 10.2514/1.J051702